PROCEEDINGS, 41st Workshop on Geothermal Reservoir Engineering
Stanford University, Stanford, California, February 22-24, 2016
SGP-TR-209

Multi-scale evaporator architectures for geothermal binary power plants

Adrian S. Sabau[1], Ali H. Nejad[2], James W. Klett[1], Adrian Bejan[3], and Kivanc Ekici[2]

[1]Oak Ridge National Laboratory, Materials Science and Technology Division, Oak Ridge, TN 37830, USA

[2]Mechanical Aerospace and Biomedical Engineering Department, The University of Tennessee, Knoxville, TN 37996-2210

[3]Duke University, Durham, NC 27708-0300, U.S.A

sabaua@ornl.gov

Keywords: Heat Exchanger, Binary cycle, Organic Rankine Cycle, Supercritical

ABSTRACT

In this paper, novel geometries of heat exchanger architectures are proposed for evaporators that are used in Organic Rankine Cycles. A multi-scale heat exchanger concept was developed by employing successive plenums at several length-scale levels. Flow passages contain features at both macro-scale and micro-scale, which are designed from Constructal Theory principles. Aside from pumping power and overall thermal resistance, several factors were considered in order to fully assess the performance of the new heat exchangers, such as weight of metal structures, and total present cost. Numerical simulations based on laminar and turbulent flow correlations for supercritical R134a and water were used to obtain performance indicators for new heat exchangers and baseline heat exchangers. For some operating conditions it was found that the new heat exchangers outperform their corresponding baseline heat exchangers.

1. INTRODUCTION

Increasing the brine effectiveness for binary geothermal plants is one of the most efficient ways to lower the cost of geothermal power generation. Minimization of the temperature differences and the elimination of the "pinch points" in the boiler will lead directly to an increase in the brine effectiveness. However, these characteristics cannot be altered with the rigid flow-paths found in the traditional shell-and-tube heat exchanger designs.

In this study, the advancements made in the design of flow-paths are reviewed, and several concepts were proposed for performance evaluation. In the last two decades new flow-paths for heat exchangers that include refinement at several length scale levels was proposed (Bejan and Errera 2000; Bejan, 2002; da Silva et al. 2004; Zimparov et al. 2006). A multi-scale approach was introduced by Bejan and his collaborators in a series of papers. A multi-scale design optimization method using fractal and constructal approaches was introduced by Luo et al. 2007. It has to be mentioned that recently, several cross-flow heat exchangers were proposed (Harris et al., 2000). The envisioned evaporator designs considered include several sections, each with its own length scale. In addition to the heat load and parasitic losses, an attempt was made to estimate the cost for the new proposed heat exchanger designs.

2. HEAT EXCHANGER ARCHITECTURE AND GEOMETRY

In this study, a heat exchanger architecture that accommodates flow-paths at several length scale levels, similar to those investigated by Bejan and Errera (2000), Bejan (2002), da Silva et al. (2004), Zimparov et al. (2006), and Luo et al. (2007), is considered. A cross-flow design was chosen in order to accommodate the multiple flow paths that contain these channels at several length-scales. The heat exchanger (HX) architecture consists of a series of channels that distribute the flow to the next level of channels and so on. A schematic of the proposed heat exchanger architecture is shown in Figure 1. Consistent with geothermal evaporator designs, the brine (fluid 1) flows within the channels while the refrigerant (fluid 2) flows in the vertical direction around the 3-rd level channels and along the 2-nd level channels. Basically, the i-th level channels act as plenums for channels at level "i+1". The channels in the last level of refinement are considered to be circular pipes unlike all the channels at the other levels, which have rectangular cross-sections. In this study, three levels of channel size refinement are used, i.e., the 3-rd channel level contains features at the smallest length-scales. The length of the 3-rd level channel is equal to (or a fraction of) the thermal entrance length defined as:

$$Le_3 = 0.05\, D_3\, Re_3 Pr_1 \quad \text{for laminar flow and } Le_3 = 10\, D_3 \quad \text{for turbulent flow} \tag{1}$$

The "thermal entrance length" concept was successfully introduced in the design of a dendritic heat exchanger by Bejan (2002). A schematic of the heat exchanger architecture is shown in Figure 2 to indicate: (a) dimensions for the 1-st and 2-nd level channels, and (b) dimensions and flow patterns for 3-rd level channels. The geometry relationships across different channels are given in Table 1 for the flow path of fluid 1. Note that for the sake of simplicity, the subscripts for fluid 1 were omitted in the Table 1. The pipes are arranged in a staggered pattern (Figure 3), governed by dimensionless spacing "a" and "b" between the tubes in the direction normal to the flow and along the flow, respectively. The values in Figure 3 for the "a" and "a/b" cases, were limited by the availability of correlations for the friction coefficient and the Nusselt number through staggered tubes (Heat Exchanger Design Handbook, 1983).

The HX designs are labeled by specifying a letter (A-E) followed by 4 numbers, indicating the following variables:

- staggered mode (letter A-F as shown in Figure 3),
- n_2, number of 2-nd level channels on one horizontal row,
- ns_2 number of rows of 2-nd level channels in the vertical direction, which is effectively the number of passes of fluid 1,
- n_3 number of 3-rd level channels on one horizontal row, and
- ns_3 number of vertical rows of 3-rd level channels.

As an example, design A6_4_8_4 would indicate (1) an arrangement of tubes corresponding to the combination of a=1.5 and a/b=1.5 (actually drawn in Figure 3a), and (2) n_2=6, ns_2=4, n_3=8, and ns_3=4. The relationship between the total flow rate and that through one 3-rd level channel for the 1-st fluid, $Q_{1,ch}$, and 2-nd fluid are given by:

$$Q_{0,1} = n_2\ (2\ n_3)\ n_{s3}\ Q_{1,ch} \text{ and } Q_{0,2} = (2n_2 - 1)\ (n_3 - 1)\ Q_{2,ch}, \text{ respectively.} \quad (2)$$

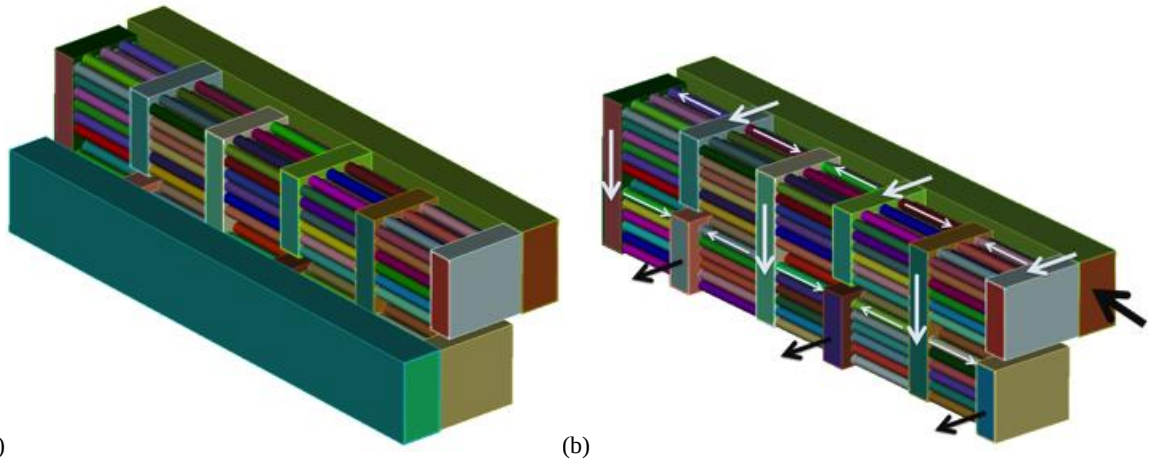

(a) (b)

Figure 1. Drawings of the tube-based heat exchanger architecture illustrating the use of channels of different lengthscale levels: (a) entire HX and (b) HX with 1-st level inlet channel removed for a detailed view of the internal.

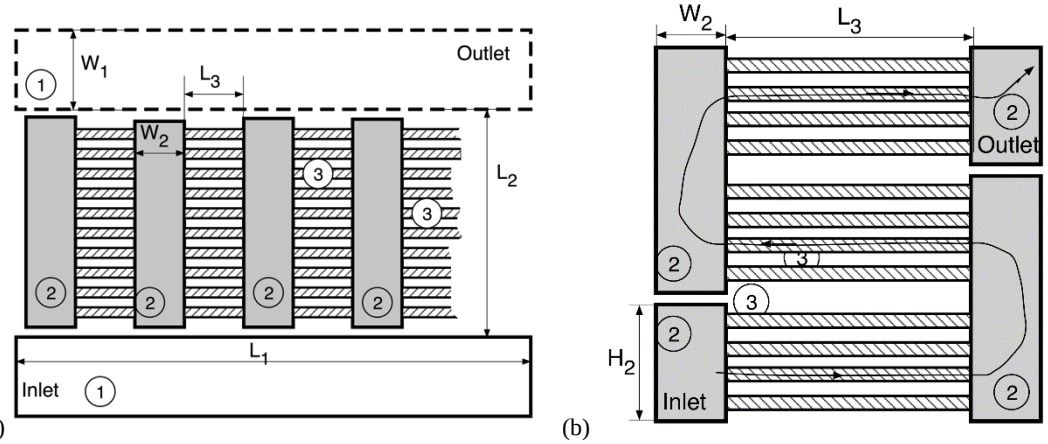

(a) (b)

Figure 2. Schematic of the tube-based heat exchanger architecture indicating dimensions for several channel levels: (a) top view of the inlet level cross-section, identifying the three channel levels (number of 3-rd levels channels n_3=10) (b) vertical cross-section illustrating ns_3=4 for the number of vertical rows of tubes and ns_2=3 for the number of vertical rows of 2-level channels.

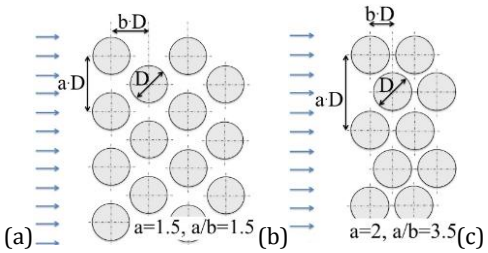

Id	a	a/b
A	1.5	1.5
B	2	1.5
C	2	2
D	2	2.5
E	2	3
F	2	3.5

Figure 3. Drawings of staggered tube arrangement for cases (a) a=1.5 and a/b=1.5; and (b) a=2 and a/b=3.5. Letter identification for all cases considered.

The optimum spacing of cooling channels and for volumetric heating was investigated in Bejan and Errera (2000). However, these optimum relationships cannot be directly used for a two-stream heat exchanger as the nature of the heat generated volumetrically in Bejan and Errera (2000) is different than the heat exchanged in two-stream heat exchangers. The relationship between the size of the channels at one level, *k*, with respect to the size of the channels at the next level, *k+1*, is based on generalization of the "Murray's law." Murray (1926) found that the optimum ratio between pipe diameters in a bifurcation joint was found to scale to $2^{1/3}$. This principle was mainly used for bifurcating channels in a general theory of multi-scale shapes and structures in nature and engineering, called the "Constructal theory" (Bejan, 1997; Ledezma et al., 1997; Bejan 2000a, Bejan, 2000b) and ramified fluid distributors (Tondeur and L. Luo, 2004). Here, it is assumed that for the case when one large channel distributes flow to identical number of multiple channels, M, a similar relationships between the channel sizes to that given by Murray's law holds, i.e.,:

$$D_{main\_channel} = D_{ch}(M)^{1/3} \tag{3}$$

Table 1. Geometry relationships across different channel levels when N=3.

Level	Relationships	Assumptions/Notes
1	$W_1 = W_2(n_2)^{1/3}$; $H_1 = H_2$ $L_1 = (2n_2 - 1)\, L_3 + 2n_2(2\, t_2 + W_2)$ $A_1 = W_{0,in}\, H_1$	Generalized Murray's law for channel size, Eq. 3 n_2 number of 2-nd channels from channel 1
2	$W_2H_2 = 0.25\pi\, W_3^2(2ns_3\, n_3)^{1/3}$; $H_2 = H_1$ $L_2 = (n_3 - 1)\, S_3 + n_3\, (2\, t_3 + W_3)$ $A_2 = W_2\, H_2$ $Q_2 n_2 = Q_1$	Generalized Murray's law for channel size, Eq. 3 ns_2 number of vertical rows of 2-nd channels n_3 number of 3-rd channels from channel 2 ns_3 number of vertical rows of 3-nd channels
3	$L_3 = Le_{1,3}$ $A_3 = 0.25\pi\, W_3^2$ $Q_3(2\, n_3)\, ns_3 = Q_2$	Entrance length, Eq. 1
0	$L_0 = W_{0,in} + W_{0,out} + L_2$ $W_0 = L_1$ H_0 – height	Neglecting wall thicknesses of inlet plenum and exit plenum

4. COMPUTATIONAL METHODOLOGY FOR THE ANALYSIS OF TEMPERATURE AND PRESSURE DROP

In order to account for the variation of the heat transfer coefficient in the entrance region, a heat transfer model was developed. The variation of the brine and refrigerant temperatures along each pipe was considered. For the sake of simplicity, the temperature within each pipe in the same horizontal plane was considered to be the same. The temperature properties of the R134a refrigerant and brine (water) were calculated using the REFPROP database. The inlet temperatures for the brine and refrigerant were 160 and 25 ^{o}C, respectively. The inlet pressure for the brine and refrigerant were considered to be 1.5 and 5.09 MPa, respectively. Each pipe was discretized into a number of segments in order to capture the variation in fluid properties and temperatures were calculated at these locations. The computational cycle and equations used for temperature calculations are shown in Table 2.

Table 2. Overall computational cycle for temperature calculations.

Start solver for dimensions

1) Obtain L_3 based on the channel flow rate and fluid properties (Eq. 1)
2) Obtain all other geometry dimensions using relationships in Table 1.

End dimension solver.
Start loop for each segment along the pipes
Start iteration, *m*

1) Calculate inside fluid 1 properties at $T_1^{ave} = 0.5\left(T_1^{in} + T_1^{out}\right)$ and Pr, Re, Nu, and h_1
2) Calculate temperature at the segment exit for the inside fluid, $T_1^{new,out}$, using T_2^{ave} at previous iteration.

$$T_1^{new,out} = T_2^{ave} - \left(T_2^{ave} - T_1^{in}\right) \exp\left(- \frac{2\pi r_o}{Q_{1,ch}\, C_{p1} \left[\frac{1}{h_1} + \frac{r_i}{k_s}\log\left(\frac{r_o}{r_i}\right) + \frac{r_i}{r_o}\frac{1}{h_2}\right]} \Delta L \right)$$

3) Calculate the heat exchanged for inside fluid, as:

$$q_1 = Q_{1,ch}\, Cp_1 \left(T_1^{new,out} - T_1^{in}\right)$$

4) Calculate the outside fluid temperature based on the energy balance:

$$q_1 = Q_{2,ch}\, Cp_2 \left(T_2^{new,out} - T_2^{in}\right)$$

5) Calculate the outside wall temperature based on heat flux and thermal resistance from the refrigerant to the outside wall.

$$T_{wall,2}^{new} = T_1^{out} + \frac{q_1}{\pi D_3\, \Delta L}\left[\frac{1}{h_1} + \frac{r_i}{k_s} log\left(\frac{r_o}{r_i}\right)\right]$$

6) Calculate $Pr_{wall,2}$ at $T_{wall,2}^{new}$
7) Calculate outside fluid properties at $T_2^{ave} = 0.5\left(T_2^{in} + T_2^{out}\right)$ and Pr, Re, Nu, and h_2
8) Evaluate the residual between the temperatures at previous cycle and current cycle,

$$|res| = ABS\left(1 - {T_{wall,2}^{new}}/{T_{wall,2}}\right)$$

9) Exit cycle if temperature residual is less than 10^{-5}.

End cycle.
End loop for all the segments.

RESULTS

The performance of the entire HX is evaluated by the number of heat transfer units (NTU), HX effectiveness, mass of metal, area of heat exchange, total volume footprint, heat load, pressure drops for both fluids, and required pumping power for both fluids (Appendix B). In addition, total present cost, C_{tot}, is estimated based on capital investment costs, C_{init}, and discounted operating costs C_{oper} for the pumping power, as:

$$C_{tot} = C_{init} + C_{oper} \tag{4}$$

$$C_{init} = 8{,}000 + 259.2\left(A_m\right)^{0.91} = 8{,}000 + 259.2\left(\frac{mass_m}{r_m t_m}\right)^{0.91} \tag{5}$$

$$C_{oper} = \left(\frac{Q_{0,1}}{r_1}\Delta P_1 + \frac{Q_{0,2}}{r_2}\Delta P_2\right)\frac{1}{h} C_{Electric}\left[\frac{\$}{kWh}\right] H_{oper}\left[\frac{h}{year}\right] \tag{6}$$

In this study, the diameter of the 3-rd level channels, D_3, was considered to be 18mm. The wall thickness of all the channels was considered to be 1mm. The following input variables are specified: (a) total flow rates for each fluid (3 and 6 kg/s for brine and R134a, respectively), (b) the tube arrangement (Figure 3a), and (c) numbers of channels n_2, ns_2, n_3, and ns_3.

Results for laminar flow regime

Six laminar cases, A4_4_75_4, B4_4_75_4, C4_4_75_4, D4_4_75_4, E4_4_75_4, F4_4_75_4 were first considered to assess optimum tube arrangements (Figure 4). The results for the Cost objective function and NTU indicate that the optimum tube arrangements are A and F, respectively. Next, 50 cases were considered for each of the tube arrangements A and F to assess the optimum number of passes for fluid 1, ns_2. For the tube arrangement, A, the following cases were considered: A4_M_150_2, A4_M_100_3, A4_M_75_4, A4_M_60_5, A4_M_50_6, A4_M_30_10, A4_M_25_12, A4_M_20_15, A4_M_15_20, and A4_M_10_30, where M was 4, 6, 8, 10, 12, and 16. Similar cases were considered for the tube arrangement type F (i.e., with a=2 and a/b=3.5). All of these cases have $n_3 * ns_3$=const., in order to maintain the same brine flow rate as given in Eq. 2. The results for different cases with different ns_2 are shown as Cost versus NTU graphs in Figures 5a and 5b for tube arrangements of type F and A, respectively. The optimum HX designs on a (Cost, NTU) graph would be located on the lower right corner of the graphs, indicating both a lower cost function and an increased thermal performance (i.e., higher NTU). As it can be seen for both tube arrangements, the cost function and NTU increase with ns_2.

Based on the data shown in Figures 5a and 5b, HX designs with ns_2=4 and 6 were considered to be optimum, i.e., attaining an acceptable level of thermal performance with lower costs.

Next, the optimal HX designs for ns_2=4 and 6 were analyzed in detail to identify the optimum number of vertical row of tubes, ns_3. For the tube arrangement of type F (Figure 6), these HX cases were considered to be F4_M_150_2, F4_M_100_3, F4_M_75_4, F4_M_60_5, F4_M_50_6, F4_M_30_10, F4_M_25_12, F4_M_20_15, F4_M_15_20, and F4_M_10_30, where M=4 and 6 for ns_2=4 and 6, respectively. The Cost and NTU data indicate that the optimum vertical row of tubes, ns_3, was 15 for both ns_2=4 and 6. As ns_3 was increased beyond 15, the NTU showed modest increases while the costs were significantly increased. These optimum cases were F4_4_20_15 and F4_6_20_15, respectively. The results for a similar sensitivity study for the tube arrangement of type A to that for type F on ns_3 are shown in Figure 7. The Cost and NTU data indicate that the optimum vertical row of tubes, ns_3, was 5 for both ns_2=4 and 6. Unlike the variation for tube arrangement type F, the NTU variation shows a local peak at ns_3=5 while Cost shows the same variation for both tube arrangements.

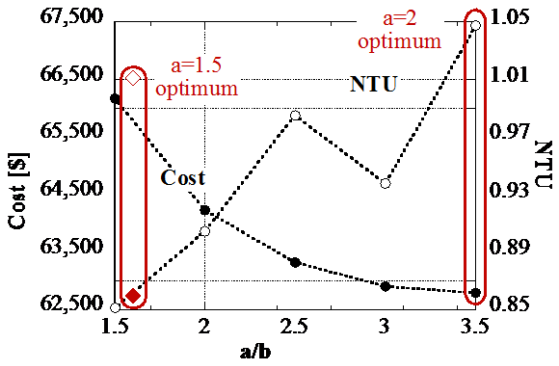

Figure 4. Calculated cost function and NTU to identify optimum arrangements for staggered pipes for laminar flows ($Q_{0,1}$=3 Kg/s and $Q_{0,2}$=6 Kg/s; n_2=4, ns_2=4, n_3=75, and ns_3=4).

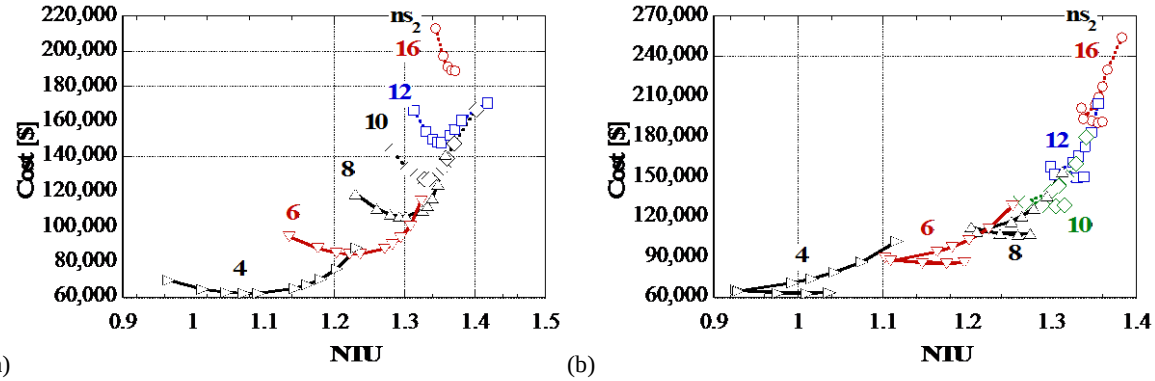

(a) (b)

Figure 5. Calculated cost function and NTU to identify optimum number of passes for fluid 1, ns_2 for laminar flows and tube arrangement types: (a) F (a=2, a/b=3.5) and (b) A (a=1.5, a/b=1.5). ($Q_{0,1}$=3 Kg/s, $Q_{0,2}$=6 Kg/s; n_2=4, n_3 and ns_3vary such that $ns_3 n_3$=const.).

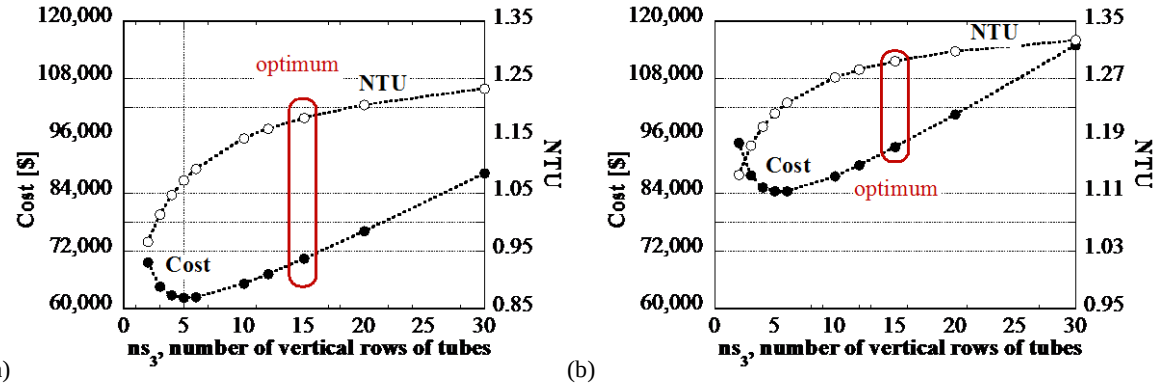

(a) (b)

Figure 6. Calculated cost function and NTU to identify optimum number of vertical row of tubes, ns_3, for laminar flows, tube arrangement type F and number of fluid 1 passes of: (a) ns_2=4 and (b) ns_2=6 (n_3 and ns_3vary such that $ns_3 n_3$=const.).

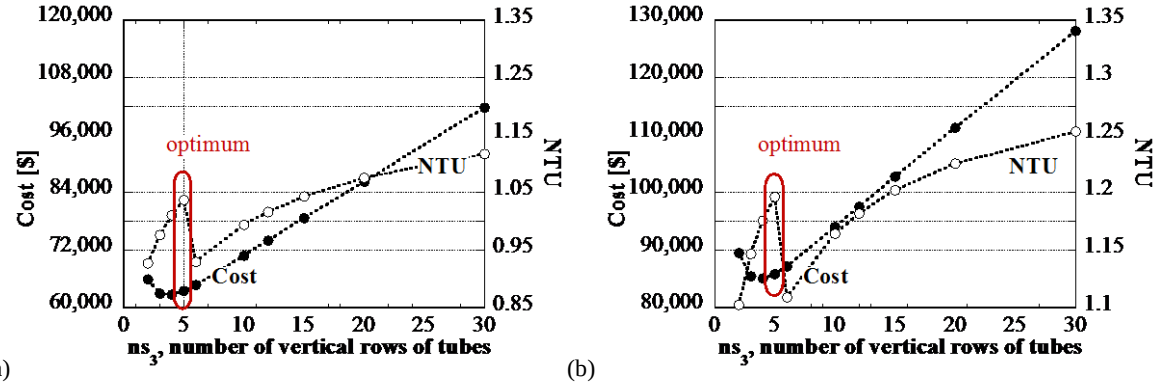

Figure 7. Calculated cost function and NTU to identify optimum number of vertical row of tubes, ns_3, for laminar flows, tube arrangement type A and number of fluid 1 passes of: (a) ns_2=4 and (b) ns_2=6 (n_3 and ns_3vary such that $ns_3 n_3$=const.).

Next, a sensitivity of the Cost function and NTU were analyzed as a function of the number of 2-nd level channels on one horizontal row, n_2. The 46 HX cases considered for this sensitivity study are shown in Table 3. For all these cases, ns_2=4. For tube arrangement type F, the results for the Cost function and NTU are shown in Figure 8a. For each n_2, the NTU increases monotonically as n_3 is decreased (and ns_3 is increased accordingly), while the cost function exhibit a local minimum. The optimum cases correspond to ns_3=6 and are highlighted and indexed in Figure 8a. These optimum cases are indicated with a * mark on Table 3 and their design labels are F4_4_50_6, F6_4_33_6, F8_4_25_6, and F10_4_20_6. For tube arrangement type A, the results for the Cost function and NTU are shown in Figure 8b. Unlike the variation for type F tube arrangement, for each n_2, the NTU exhibits an "N" type variation, peaking at ns_3=5 and at it largest value considered, and exhibiting a local minimum at ns_3=6. The cost function exhibits similar variation, showing a local minimum for moderate values of ns_3. The optimum cases correspond to ns_3=5 and are highlighted and indexed in Figure 8a. These optimum HX cases are indicated with ** mark on Table 3 and their design labels are A4_4_60_5, A6_4_40_5, F8_4_30_5, F10_4_24_5, and F12_4_20_5.

Comparison between new heat exchangers and their corresponding baselines for laminar flows

In order to assess the potential improvement of the new HX designs, baseline HX designs were investigated for a direct comparison with new HX designs. Ideally, the baseline HX designs should include long tubes of the same diameter as those of the 3-rd tubes, placed between one inlet and one outlet. The length of the baseline tube should be set to the length of horizontal entrance-length tubes on one row, as if the level 2 plenums would be simply removed. Removing the internal level 2 channels to construct the corresponding baseline HX design would have an effect of creating longer tubes, as they are now used in current practice. By removing the internal level 2 channels, the flow rate inside the tubes would increase accordingly. Here, the baseline HX designs were created starting from a new HX design by removing most of the internal level 2 plenums and keeping n_2=2. The limitation of baseline HX to configurations with n_2=2, having two inlets and two outlet plenums of level 2, is imposed by the current solver to estimate the HX performance. In the simulation of the baseline HX performance the same flow rates were used for the fluids considered. This is consistent with geothermal applications, in which the brine flow rate is usually fixed and the maximum power in geothermal systems is sought at a constant brine flow rate. The 9 cases, which were found to be optimum for the n_2 sensitivity study, were considered for evaluation against their corresponding baselines. Those cases are highlighted in Table 3 and marked with * (F4_4_50_6, F6_4_33_6, F8_4_25_6, and F10_4_20_6) and ** (A4_4_60_5, A6_4_40_5, A8_4_30_5, A10_4_24_5, and A12_4_20_5). For some baseline cases, the flow regime in the tubes changed from the laminar to the turbulent regime. For those baseline HXs, which are expected to operate in the turbulent regime, appropriate correlations for the turbulent flow were used to estimate their performance. Thus, the comparison has to be made not only between new HXs and baseline HXs operating both in the laminar flow regime, but also for cases in which the new HX are in the laminar regime and baseline HX are in the turbulent regime. The Cost function vs. NTU is shown for both the new HX and corresponding baseline HX in Figure 9. For the tube arrangement type F, the new HX exhibit the lowest cost but at average performance. The data shown in Figure 9a, indicate that the new laminar HX outperform the corresponding baseline laminar HXs that operate both in the laminar regime (i.e., having higher performance at lower cost). For those baseline turbulent HX cases, the comparison with the corresponding new HX is not straightforward. Those laminar HXs are still lest costly but their performance is reduced as compared to their corresponding baseline HXs. For the tube arrangement type A, the new HXs outperform the corresponding baseline laminar HXs and baseline turbulent HXs, as their cost function is the lowest while the NTU performance is almost identical to the baseline HX (turbulent or laminar).

Table 3. HX designs for laminar regime showing considered n_3 number of 3-rd channels on one horizontal row, and ns_3 number of vertical rows of 3-rd channels for different numbers of 2-nd level channels on one horizontal row, n_2 (ns_2=4).

n_2=4			n_2=6			n_2=8			n_2=10			n_2=12		
case	n_3	ns_3	case	n_3	ns_3	case	n_3	ns_3	case	n_3	ns_3	case	n_3	ns_3
1	150	2	12	100	2	23	75	2	33	60	2	43	50	2
2	100	3	13	66	3	24	50	3	34	40	3	44	33	3
3	75	4	14	50	4	25	37	4	35	30	4	45	25	4
**4	60	5	**15	40	5	**26	30	5	**36	24	5	**46	20	5
*5	50	6	*16	33	6	*27	25	6	*37	20	6	47	16	6
6	30	10	17	20	10	28	15	10	38	12	10	48	10	10
7	25	12	18	16	12	29	12	12	39	10	12	49	8	12
8	20	15	19	13	15	30	10	15	40	8	15	50	6	15
9	15	20	20	10	20	31	7	20	41	6	20			
10	10	30	21	6	30									

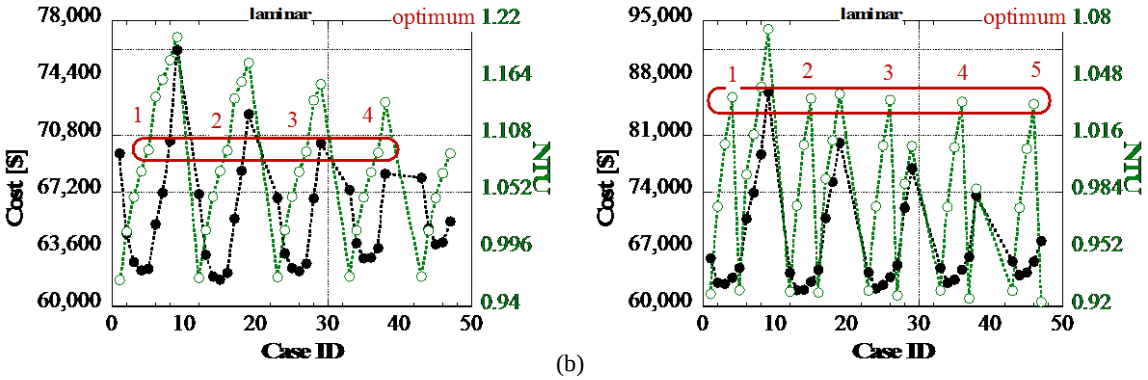

(a) (b)

Figure 8. Calculated cost function and NTU to identify optimum numbers of 2-nd level channels on one horizontal row, n_2, for laminar flows and tube arrangement types: (a) F (a=2, a/b=3.5) and (b) A (a=1.5, a/b=1.5). ($Q_{0,1}$=3 Kg/s, $Q_{0,2}$=6 Kg/s; ns_2=4; n_3 and ns_3 as shown in Table 3).

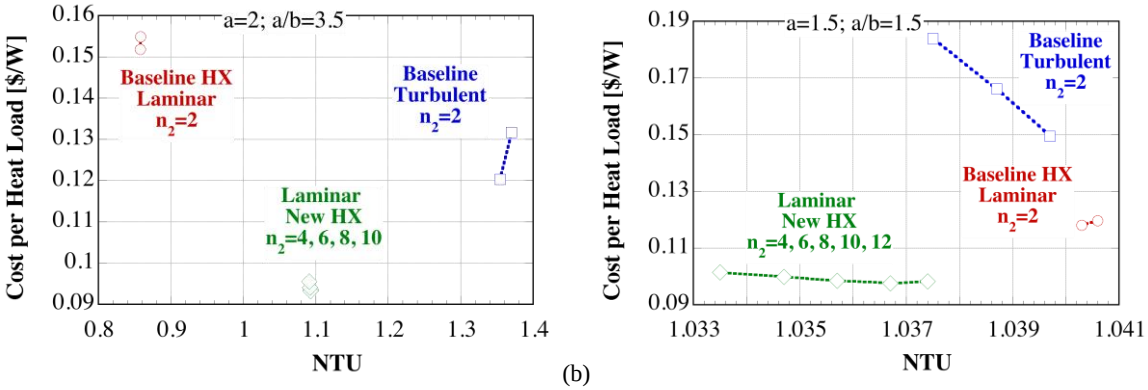

(a) (b)

Figure 9. Calculated cost function per heat load and NTU for several new HX designs and their corresponding baseline HX designs for laminar flows and tube arrangement types: (a) F and (b) A. ($Q_{0,1}$=3 Kg/s, $Q_{0,2}$=6 Kg/s).

Results for turbulent flow regime

For the turbulent flow regime, a similar approach to that for the laminar regime was taken. Although not shown here, similar results to those presented in Figure 5 indicated that ns_2=12 is optimum for the turbulent HXs. A sensitivity of the Cost function and NTU were analyzed as a function of the number of 2-nd level channels on one horizontal row, n_2. The 35 HX cases considered for this sensitivity study are shown in Table 4. For all these cases, ns_2=12. For tube arrangement type F, the results for the Cost function and NTU are shown in Figure 10a. For each n_2, the NTU increases monotonically as n_3 is decreased (and ns3 is increased accordingly), while the cost function exhibit a local minimum. The optimum cases correspond to ns_3=6. These optimum cases are indicated with * on Table 4 and their design labels are F6_12_33_6, F8_12_25_6, and F10_12_20_6. For tube arrangement type A, the results for the Cost function and NTU are shown in Figure 10b. Unlike the variation for the laminar flow, for type F tube arrangement, the NTU increases

monotonically. The cost function exhibits similar variation, showing a local minimum for moderate values of ns_3. The optimum cases correspond to ns_3=6. These optimum HX cases are indicated with * on Table 4 and their design labels are A6_12_33_6, A8_12_25_6, and A10_12_20_6.

Comparison between new heat exchangers and their corresponding baselines for turbulent flows

In order to assess the potential improvement of the new HX designs, baseline turbulent HX designs were investigated for a direct comparison with new turbulent HX designs. Ideally, the baseline HX designs should include long tubes of the same diameter as those of the 3-rd tubes, placed between one inlet and one outlet. As indicated in the laminar flow sections, the baseline HX designs were created starting from a new HX design by removing most of the internal level 2 plenums and keeping n_2=2. The limitation of baseline HX to configurations with n_2=2, having two inlets and two outlet plenums of level 2, is imposed by the current solver to estimate the HX performance. In the simulation of the baseline HX performance the same flow rates were used for the fluids considered. The 3 cases, which were found to be optimum for the n_2 sensitivity study, were considered for evaluation against their corresponding baselines. Those cases are highlighted in Table 3 were F6_12_33_6, F8_12_25_6, and F10_12_20_6. The Cost function vs. NTU is shown for both the new HX and corresponding baseline HX in Figure 11 for the tube arrangement type F, the new HX exhibit the lowest cost but lower thermal performance than their corresponding turbulent baseline HXs. Definitely, if cost would be the ultimate selection criteria, then the new turbulent HX would be desired.

Table 4. HX designs for turbulent regime showing considered n_3 number of 3-rd channels on one horizontal row, and ns_3 number of vertical rows of 3-rd channels for different n_2 numbers of 2-nd level channels on one horizontal row (ns_2=12).

n_2=6			n_2=8			n_2=10			n_2=12		
case	**n_3**	**ns_3**	**case**	**n_3**	**ns_3**	**case**	**n_3**	**ns_3**	**case**	**n_3**	**ns_3**
1	100	2	12	75	2	22	60	2	32	50	2
2	66	3	13	50	3	23	40	3	33	33	3
3	50	4	14	37	4	24	30	4	34	25	4
4	40	5	15	30	5	25	24	5	35	20	5
*5	33	6	*16	25	6	*26	20	6	36	16	6
6	20	10	17	15	10	27	12	10	37	10	10
7	16	12	18	12	12	28	10	12	38	8	12
8	13	15	19	10	15	29	8	15	39	6	15
9	10	20	20	7	20	30	6	20			
10	6	30									

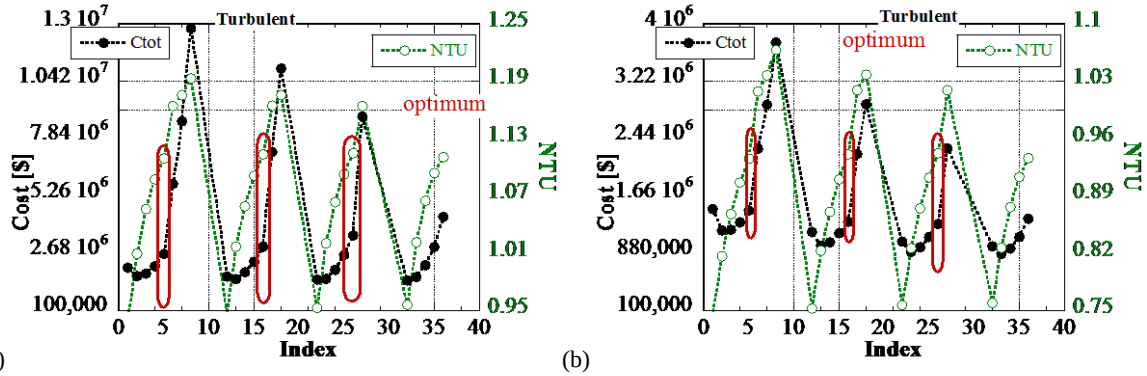

(a) (b)

Figure 10. Calculated cost function and NTU to identify optimum numbers of 2-nd level channels on one horizontal row, n_2, for turbulent flows and tube arrangement types: (a) F (a=2, a/b=3.5) and (b) A (a=1.5, a/b=1.5). ($Q_{0,1}$=20 Kg/s, $Q_{0,2}$=40 Kg/s; ns_2=12; n_3 and ns_3 as shown in Table 4).

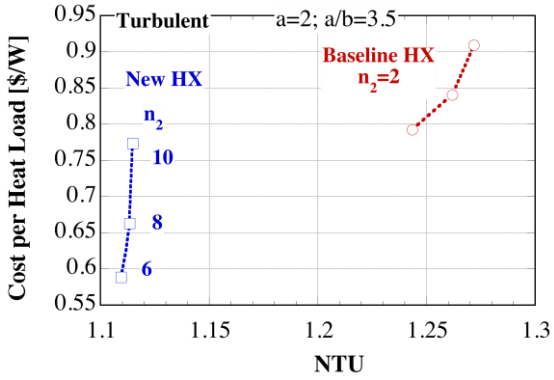

Figure 11. Calculated cost function per unit load and NTU for several new HX designs and their corresponding baseline HX designs for turbulent flows. Tube arrangement types F ($Q_{0,1}$=20 Kg/s, $Q_{0,2}$=40 Kg/s).

CONCLUSIONS AND DISCUSSIONS

A cross-flow heat exchanger design was chosen in order to accommodate the multiple flow paths that contain these channels at several length-scales. The HX architecture consists of a series of channels that distribute the flow to the next level of channels and so on. Basically, the i-th level channels act as plenums for channels at level "i+1". The channels in the last level of refinement are considered to be circular pipes unlike all the channels at the other levels, which have rectangular cross-sections. The relationship between the size of the channels at one level, *k*, with respect to the size of the channels at the next level, *k+1*, is based on generalization of the "Murray's law." In order to account for the variation of the temperature and heat transfer coefficient in the entrance region, a heat transfer model was developed. The variation of the brine and refrigerant temperatures along each pipe was considered.

The performance of the entire HX was evaluated by several indicators, including the number of heat transfer units (NTU), HX effectiveness, mass of metal, area of heat exchange, total volume footprint, heat load, pressure drops for both fluids, and required pumping power for both fluids. In addition, total present cost, which was estimated based on capital investment costs and discounted operating costs for the pumping power, was calculated. For the laminar and turbulent flows, the results for the Cost objective function and NTU were used to identify the optimum tube arrangements. For laminar flow, it was found that the optimum numbers of passes were 4 and 6. Depending on the tube arrangement, it was found that the optimum number of vertical rows, which is in fact number of rows in the tube bank seen by the outside fluid, was either 5 or 15.

In order to assess the potential improvement of the new HX designs, baseline HX designs were investigated for a direct comparison with new HX designs. Ideally, the baseline HX designs should include long tubes of the same diameter as those of the 3-rd tubes, placed between one inlet and one outlet. The baseline HX designs were created from the new HX designs by simply removing most of the internal 2-nd level channels to use longer tubes than the entrance length, as they would currently be used. Consistent with geothermal applications, the performance of new HX designs was compared to that of baseline HX designs at the same flow rates. For some baseline cases, the flow regime in the tubes changed from the laminar (for the original new HX) to the turbulent regime. For the tube arrangement type F, the Cost function and NTU data indicate that the new laminar HXs outperform the corresponding baseline laminar HXs that operate both in the laminar regime (i.e., having higher performance at lower cost). For those baseline turbulent HXs, which originate from laminar new HXs, the comparison with the corresponding new HX is not straightforward. Those laminar HXs are still lest costly but their performance is reduced as compared to their corresponding baseline HXs. For the tube arrangement type A, the new HXs outperform the corresponding baseline laminar HXs and baseline turbulent HXs, as their cost function is the lowest while the NTU performance is almost identical to the baseline HX (turbulent or laminar).

For the turbulent flow regime, a similar approach to that for the laminar regime was taken. For turbulent flows, it was found that the optimum number of vertical rows, i.e., number of rows in the tube bank seen by the outside fluid, was 6. For the tube arrangement type F, the Cost function vs. NTU data for both the new HX and corresponding baseline HX, showed that the new HX exhibit the lowest cost but lower thermal performance than their corresponding turbulent baseline HXs. In these cases, it is still an open question how the thermal performance as defined by NTU would impact the selection of costlier HXs. Definitely, if cost would be the ultimate selection criteria, the new turbulent or laminar heat exchanger would be desired.

ACKNOWLEDGEMENT

This work was performed for the project "Freeform Heat Exchangers for Binary Geothermal Power Plants" sponsored by the Geothermal Technologies Program, Office of Energy Efficiency and Renewable Energy, U.S. Department of Energy under contract DE-AC05-00OR22725, Oak Ridge National Laboratory, managed and operated by UT-Battelle, LLC.

REFERENCES

A. Bejan, Dendritic constructal heat exchanger with small-scale crossflows and larger-scales counterflows, International Journal of Heat and Mass Transfer, Volume: 45, pp. 4607-4620, 2002.

L. Luo, Y. Fan, D. Tondeur, Heat exchanger: from micro-to multi-scale design optimization, International Journal of Energy Research 31 (13), 1266-1274, 2007.

V.D. Zimparov, A.K. da Silva, A. Bejan, Constructal tree-shaped parallel flow heat exchangers, International Journal of Heat and Mass Transfer, Volume 49, 2006, Pages 455–4566

A. Bejan and Errera, MR, Convective trees of fluid channels for volumetric cooling, International Journal of Heat and Mass Transfer, Volume 43 pp: 3105-3118, 2000.

A.K. da Silva, S. Lorente, A. Bejan, Constructal multi-scale tree-shaped heat exchangers, Journal of Applied Physics 96, 1709 (2004).

S.G. Kandlikar, S. Garimella, D. Li, S. Colin, M.R. King, Heat Transfer and Fluid Flow in Minichannels and Microchannels, Elsevier, Inc.,1-st edition, 2006.

D. Tondeur and L. Luo, Design and scaling laws of ramified fluid distributors by the constructal approach, Chemical Engineering Science, Volume 59, 2004, pp. 1799–1813.

C.D. Murray, The physiological principle of minimal work, in the vascular system, and the cost of bloodvolume, Proc. Acad. Nat. Sci. 12 (1926) 207–214.

A. Bejan, From heat transfer principles to shape and structure in Nature, Journal of Heat Transfer, Transactions of ASME 122, 2000a. 430–449.

A. Bejan, Shape and Structure, from Engineering to Nature, Cambridge University Press, Cambridge, UK, 2000b.

A. Bejan and S. Lorente, The constructal law and the thermodynamics of flow systems with configuration, International Journal of Heat and Mass Transfer 47 (2004) 3203–3214.

G. Ledezma, A. Bejan, and M.R. Errera, 1997. Constructal tree networks for heat transfer. Journal of Applied Physics 82, 89–100.

Heat Exchanger Design Handbook (1983) Hemisphere, New York, 1983. DOI: 10.2514/3.60159

A.C. Caputo, P.M. Pelagagge, and P. Salini, Heat exchanger design based on economic optimisation, Applied Thermal Engineering, Volume 28, 2008, Pages 1151–1159.

A. Bejan, Convection Heat Transfer, 3rd ed., John Wiley and Sons, Inc., Hoboken, NJ (2004).

R.K. Shah, A Correlation for Laminar Hydrodynamic Entry Length Solutions for Circular and Noncircular Ducts, J. Fluids Eng. 100, 177-179, 1978.

APPENDIX A.

Correlations for fluid dynamics and heat transfer in the entrance region of a tube and for flow through a tube bank

The average Nusselt number, between x_1 and x_2 locations away from the entrance, within the entrance region for a tube is given (Bejan, 2004), as:

$$\overline{\mathrm{Nu}} = \frac{1}{x_2 - x_1}\int_{x_1}^{x_2} \mathrm{Nu}_x \, dx = \frac{1}{x_2 - x_1}\left[3.1815\left(\sqrt{\frac{x}{RePrD_3}}\right)^{0.3178}\right]_{x_1}^{x_2} \tag{A1}$$

The average heat transfer coefficient over the entrance region becomes:

$$h_1 = \frac{\overline{Nu}\, k_1}{D_{h,3}} \text{ and } h_2 = \frac{\overline{\mathrm{Nu}}\, k_2}{D_{h,3b}} \tag{A2}$$

The overall heat transfer coefficient between fluids 1 and 2 in the level 3 channels is then given by:

$$\bar{h} = \frac{1}{\frac{1}{h_1} + \frac{t_3}{k_s} + \frac{1}{h_1}} \tag{A3}$$

The following correlation was used for the Nusselt number for the flow through a staggered bank of tubes (Bejan, 2004):

$$\overline{Nu} = 0.9\, C_n \mathrm{Re}^{0.4} Pr_b^{\,0.36}\left(\frac{Pr_b}{Pr_{b,w}}\right)^{0.25}, \tag{A4}$$

where Reynolds number, $\mathrm{Re} = \frac{V_{max} D_o}{\upsilon}$, for the outside fluid is based on the maximum velocity through the tube banks, which occurs at the smallest cross sectional area between the tubes. Where $Pr_{b,w}$ is evaluated at wall temperature.

The pressure drop in the entrance region of a pipe was estimated using the relationships from Shah (1978), as:

$$\Delta P = f_{app} Re\ 4\ x^+ \frac{\rho u^2}{2};\ f_{app} Re = \frac{3.44}{\sqrt{x^+}} + \frac{f\ Re + K(\infty)/4x^+ + 3.44/\sqrt{x^+}}{1 + C\ (x^+)^{-2}};\ x^+ = \frac{x}{Re\ D} \tag{A5}$$

The pressure drop in a tube bank was computed, as:

$$\Delta P = EuK_1 * \alpha\left(\frac{a}{b}\right)^{\beta} * ns_2 * ns_3 * \frac{\rho_2 {V_{max}}^2}{2} \tag{A6}$$

Table A1. Correlations for α and β coefficients used to estimate the pressure drop in a tube bank.

a/b	Re	α	β
0.5 to 1.2	50 to 2,000	1	$0.096 - 0.048 * \log10(Re)$
1.25 to 3.5	50 to 2,000	$0.888 + 0.021 * \log10(Re)$	$0.872 - 0.196 * \log10(Re)$

Table A3. Correlations for EuK_1 used to estimate the pressure drop in a tube bank.

a	Expression for EuK_1
a < 1.375	$EuK_1 = 0.795 + \frac{0.247E3}{Re} + \frac{0.335E3}{Re^2} - \frac{0.155E4}{Re^3} + \frac{0.241}{Re^4}$
a > 1.375 and a < 1.75	$EuK_1 = 0.683 + \frac{0.111E3}{Re} - \frac{0.973E2}{Re^2} + \frac{0.426E3}{Re^3} - \frac{0.574E3}{Re^4}$
a>1.75	$EuK_1 = 0.713 + \frac{0.448E2}{Re} - \frac{0.126E3}{Re^2} - \frac{0.582E3}{Re^3}$

APPENDIX B.

Relationships for estimating performance of heat exchangers

The pressure drop in the entrance regions of 3-rd level channels was estimated based on the apparent friction coefficient defined in relationship A5 and the loss coefficient due to abrupt cross-section contraction at the entrance and abrupt change in cross-section at exit,

as:

$$\Delta p_1 = \frac{2\, f_{app} Re_1\, \mu_1 V_3 L_3}{{D_{h,3}}^2} + K_c \frac{\rho_1 {V_3}^2}{2} \text{ and } \Delta p_2 = \frac{2\, f_{app} Re_2\, \mu_2 V_{2,ch} H_3}{{Dh_{h,3b}}^2} \quad \text{(B1)}$$

The following relationships were then used to estimate the UA, NTU, and efficiency, as:

$$UA = \frac{Q_{avg}}{F\,\Delta T_{lm}};\; NTU = \frac{UA}{\min(C_c, C_h)};\; \varepsilon = \frac{Q_{avg}}{Q_{max}} \quad , \quad \text{(B2)}$$

where $Q_{avg} = (Q_c + Q_h)/2$; $C_c = \dot{m}_{o,ch} Cp_o$; $C_h = \dot{m}_{i,ch} Cp_i$, $Q_{max} = \min(C_c, C_h)\ (T_{i,1} - T_{o,2})$; $C_r = \min(C_c, C_h)/\max(C_c, C_h)$; and $\Delta T_{lm} = \left[(T_{i,1} - T_{o,2}) - (T_{i,2} - T_{o,1})\right] / \ln\left(\frac{T_{i,1} - T_{o,2}}{T_{i,2} - T_{o,1}}\right)$.